



ISSN 1110-0451



(ESNSA)

## Comparative study of synthesized Kaolinite supported-metal oxides for Th(IV) adsorption

Amira A. Elabd and Olivea A. Elhefnawy\*

Safeguards and Physical Protection Department, Nuclear and Radiological Safety Research Center (NRSRC), Egyptian Atomic Energy Authority, Cairo, Egypt

### ARTICLE INFO

#### Article history:

Received: 6<sup>th</sup> May 2023

Accepted: 31<sup>st</sup> May 2023

Available online: 14<sup>th</sup> Sept. 2023

#### Keywords:

Modified kaolinite;

CuO;

ZnO;

Thorium adsorption;

Batch technique;

Isothermal;

Kinetics;

Thermodynamics.

### ABSTRACT

Egyptian natural kaolinite was supported with metal oxides ZnO and CuO to prepare modified kaolinite KCu and KZn for Th(IV) adsorption from an aqueous solution. Different analyses such as SEM, EDX, XRD, and FTIR described the morphology and structural characteristics of the new adsorbents KCu and KZn. The adsorption process was applied in batch experiments as a function of pH, contact time, initial Th(IV) concentration, temperature, regeneration, and reusability. The equilibrium stage was achieved at 120 min. Experimental data were well described by the pseudo-second-order and Langmuir models with maximum adsorption capacities of 62.89 and 56.179 mg/g for KCu and KZn, respectively. Thermodynamic parameters were calculated and proved the spontaneous and endothermic nature of the adsorption process, which showed that the modified kaolinite is sensitive to temperature. Thermodynamics studies confirmed that adsorption is feasible and spontaneous. The regeneration and reusability study showed that KCu and KZn are economically viable.

## 1. INTRODUCTION

Thorium is a radioactive fissionable element used widely in different nuclear industries and research studies related to the development of thorium through the mining of rare earth elements, nuclear waste management as well as production of radioactive medical products. As a result of nuclear applications, the most significant issue is the removal of radioactive elements from the environment that cause high threats to the local ecology and human health [1,2]. Therefore, the effective recovery of thorium from wastewater before discharge has high importance to release radioactive pollution for environmental concerns [3]. A variety of mature techniques have been used to remove thorium from wastewater including solvent extraction [4,5], ion exchange [6], membrane separation [7], electrolysis [8], and adsorption [9,10]. The adsorption method has received much attention due to its high efficiency, easy operation, no environmental hazards, and high stability [11, 12]. Kaolinite is one of the most abundant components of soil structure. It is also considered one of the most suitable adsorbents due to its layered structure, strong chemical and thermal stability. Kaolinite is a

hydrated aluminum silicate structure  $Al_2Si_2O_5(OH)_4$  with a basic unit 1:1 layer structure ratio consisting of two different aluminosilicate surfaces, one of a tetrahedral silicate sheet and the other is an octahedral aluminum sheet [13]. The two sheets coordinate by hydrogen bonds between oxygen ions in one sheet with hydroxyl groups in the next. Kaolinite has a hydroxyl surface that gives it highly favorable adsorption properties indicating that it isn't inner adsorbent and has a slight negative charge [14]. There are several previous reports the treatment of kaolinite with different acids and alkalis to develop its structure and increase the adsorption capacities [15]. In this work, kaolinite was modified by doping individually metal-oxides, ZnO and CuO. Modified kaolinites have been characterized and applied for Th(IV) adsorption from aqueous solutions. Kinetics, isothermal and thermodynamic models were applied to the adsorption of Th(IV) onto the two modified kaolinites.

## 2. MATERIAL AND METHODS

Copper nitrate and Zinc nitrate were supplied by (Rankem Company). 25%  $NH_4OH$  solution was manufactured by (Merck Company). HCl,  $HNO_3$ , and

KOH were purchased from (Fisher Chemicals Company). Egyptian natural kaolinite was supplied by Sinai Manganese Company in Egypt. Thorium salt  $[\text{Th}(\text{NO}_3)_4 \cdot 4\text{H}_2\text{O}]$  was supplied by the Mallinckrodt company. Thorium solution was measured by UV-Visible Spectrophotometer (Thermo-Evolution 300, England), at a wavelength of 665 nm. The pH values were measured by Jenway 3510 pH meter. Scanning electron microscopy SEM used to investigate the surface morphology of the modified kaolinites using (ZIESS Gemini, Sigma 300 VP). Energy-dispersive X-ray detector EDX was used to carry out the elemental analysis of the modified kaolinites by JEOL, 6510 LA and to investigate the distribution of Zn and Cu on the surface of modified kaolinites KZn and KCu, respectively. X-ray powder diffraction technique was used to verify the structure and purity of the modified kaolinite by PANalytical apparatus with X'pert PRO software. Fourier transforms infrared (FTIR) spectra were used to identify the chemical structures of the modified kaolinites by the FTIR system (Shimadzu 8001, Japan).

### 2.1. Preparation of Modified Kaolinite KCu and KZn

Add 5 g of Egyptian natural kaolinite to 100 ml of 1M salt solution of  $\text{Zn}(\text{NO}_3)_2/\text{Cu}(\text{NO}_3)_2$ . The initial pH of the solution was adjusted to 12 by dropwise addition of  $\text{NH}_4\text{OH}$  solution with continued stirring for 3 h at 60 °C. The kaolinite was immersed into the working solution overnight. The modified kaolinite was washed well with

deionized water, calcined at 700 °C for 2 h, then stored for further experiments. Modified kaolinites (KZn and KCu) were characterized to investigate their composition.

### 2.2. Batch Sorption Experiments

The adsorption capacity (mg/g) at time  $t$  (min), distribution coefficient  $K_d$ , and removal efficiency  $R$  % were calculated using the following equations [16]:

$$q_t = \frac{(C_0 - C_t)V}{m} \quad (1)$$

$$K_d = \frac{(C_0 - C_e)V}{C_e m} \quad (2)$$

$$R \% = \frac{C_0 - C_t}{C_0} \times 100\% \quad (3)$$

Where  $C_0$  and  $C_t$  are the concentrations (mg/L) at  $t=0$  and ( $t$ ) time, respectively.  $V$  (L) is the volume of Th(IV) solution and  $m$  (g) is the mass of adsorbent KCu / KZn.

## 3. RESULTS AND DISCUSSION

### 3.1. Characterization

The surface morphology of the modified kaolinites KZn and KCu was described by SEM analyses and shown in Fig. 1(a, b), respectively. Figure 1 shows a porous surface of both new adsorbents. The elemental analysis of the modified kaolinite KZn and KCu was carried out by EDX analysis and shown in Fig. 2(a, b), respectively. EDX spectra confirm the successful modification of kaolinite by distributing Zn and Cu on the surface of kaolinite, respectively.

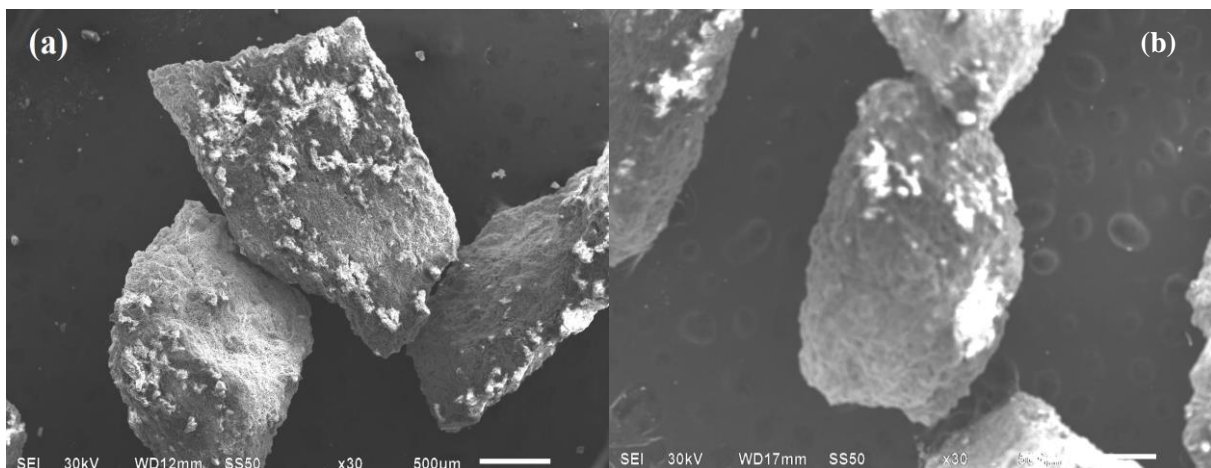


Fig. (1): SEM images of the new adsorbents (a) KCu and (b) KZn

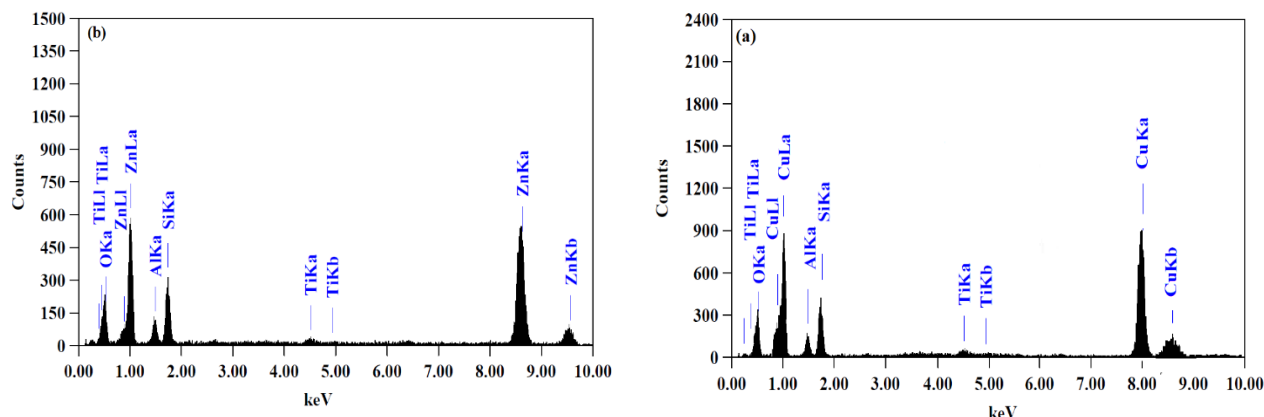


Fig. (2): EDX spectra of the new adsorbents (a) KCu and (b) KZn

Figure 3 (a, b, c) shows the FTIR infrared spectrum of the natural kaolinite before and after modification, which represents bands at the range of  $3724$  to  $3617\text{ cm}^{-1}$  are related to the stretching vibration of hydroxyl (OH) group on the external surface of the kaolinite. The bending vibration of hydroxyl groups in kaolinite are found in small peaks at range of  $1670$  -  $1487\text{ cm}^{-1}$ . While the inner (OH) as a bridge between Al and Si on the layers of the kaolinites locates at  $918\text{ cm}^{-1}$ . Fig. 3(a) represents the FTIR spectrum of the natural kaolinite. It is clear that natural kaolinite contains small organic impurities, which appear at the bands range  $2389$  and  $2278\text{ cm}^{-1}$  [15]. The broad vibration bands between  $1128$  and  $1000\text{ cm}^{-1}$  are indicated as the stretching vibration mode of the symmetrical bridge (Si-O-Si) and unsymmetrical bridge (Al-O-Si) of the natural kaolinite and unsymmetrical bridge (Cu-O-Si) and (Zn-O-Si) of the metal oxide after modifications. While the slight shift in the bands in the region of  $823$  and  $666\text{ cm}^{-1}$  are due to the formation of new bonds between Cu-O and Zn-O and the skeleton of kaolinite (Si-O), (Al-O) after modifications. Also, the peaks in the range of  $534$  to  $419\text{ cm}^{-1}$ , is related to the well-formed crystalline phase of silica in tetrahedral coordination concerning oxygen [ $\text{SiO}_4$ ]. FTIR spectra prove modification of natural kaolinite by metal oxides CuO and ZnO.

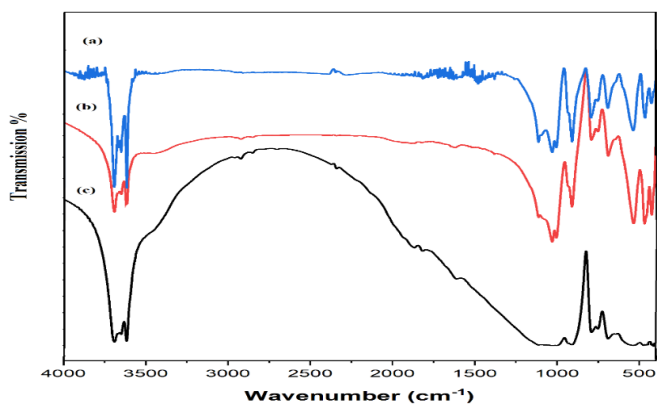


Fig. (3): FTIR spectra of the modified kaolinite (a) Natural Kaolinite, (b)KZn, and (c) KCu

XRD spectra show the structure of kaolinite before and after the modification, as shown in Fig. 4 (a, b, c). The group of bands in the range of  $2\theta = 20^\circ$ – $30^\circ$  and  $50.18^\circ$  are related to the kaolinite structure as seen in fig. 4. The sharp bands of the kaolinites before and after modification indicate their crystalline nature. Fig. 3(A) shows the sharp peaks at  $2\theta = 35.42^\circ$ ,  $36.38^\circ$ , and  $38.60^\circ$  related to the addition of ZnO in the modified kaolinite (KZn) according to the literature [JCPDS (36-1451)] [16]. Fig. 4(B) shows the sharp peaks at  $2\theta = 36.71^\circ$  and  $43.59^\circ$  assigned to CuO on the surface of the modified kaolinite (KCu) agreed with the monoclinic CuO, as same as the reported data (JCPDS, File No. 01-080-1916) [17].

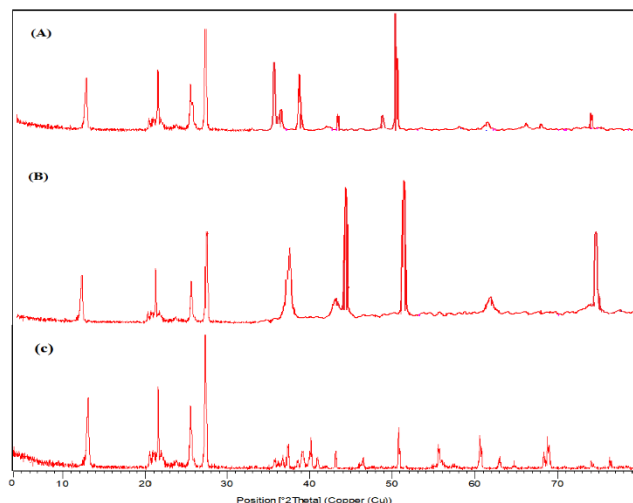
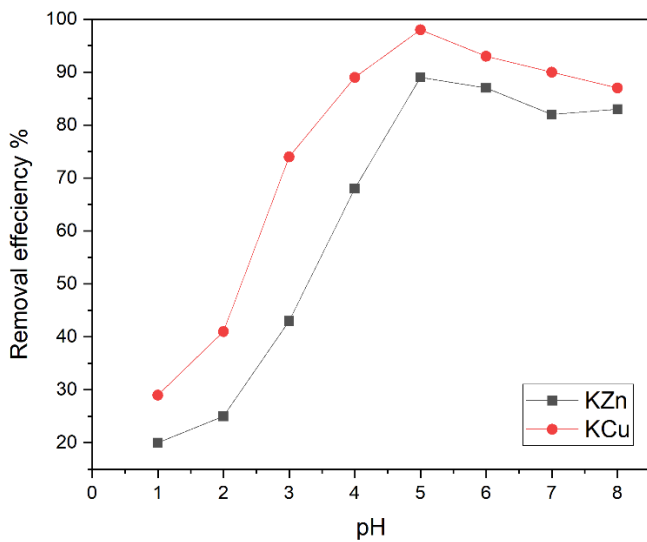


Fig. (4): XRD pattern of the new adsorbents (A) KZn, (B) KCu, and (C) Natural Kaolinite

### 3.1. The Effect of pH on adsorption process

It is substantial to study pH effects due to their significant influent on the determination of ionic species of metal cations and the ionization of functional groups of the adsorbents. The adsorption process was studied by adding  $50\text{ mg}$  of KZn / KCu to

50 ml of 30 mg/L of Th(IV) at a pH range of 1-8. Figure 5 shows the pH effect on the removal efficiency R (%) of Th(IV) on KZn and KCu. It illustrates that the R (%) increases with pH increase until it reaches a maximum at pH 5, due increase in pH will decrease protons on the surface of KZn and KCu which reduce the competition with Th (IV) cations on the active sites of KZn and KCu. While at pH > 5, the hydroxyl anions concentration will increase, and the probability of forming precipitated species Th(OH)<sub>4</sub> species will increase, which will decrease the R % of Th(IV) on KZn and KCu. Thus, pH=5 will be considered the optimum pH for further experiments.



**Fig. (5): Effect of pH on the adsorption of Th(IV) on the new adsorbents KCu and KZn**

### 3.2. The effect of contact time and kinetic study

Contact time is important to study the kinetic models of the adsorption process. The adsorption experiments were carried out at a range of contact times 1 to 200 min at 298 K. Figure 6 shows the effect of contact time on the adsorption capacity  $q_t$  (mg/g) of Th(IV) on KZn and KCu. It is clear that  $q_t$  increases with contact time increases and reaches maximum capacity  $q_e$  at 120 min. After 120 min, there is no notable change in the adsorption capacities. Thus, the adsorption capacity at 120 min will be the equilibrium capacity  $q_e = 41.23, 35.5$  (mg/g) for KCu and KZn, respectively. Thus, 120 min is considered for further experiments. The kinetic models were discussed by applying pseudo-first order and pseudo-second order to the experimental data of the adsorption process [18]. The pseudo-first order equation can be expressed as following equations:

$$\frac{dq}{dt} = K_1 (q_e - q_t) \quad (4)$$

$$\log(q_e - q_t) = \log q_e - \frac{K_1}{2.303} t \quad (5)$$

Where  $q_t$  is the adsorption capacity (mg/g) at time  $t$  (min),  $q_e$  is the adsorption capacity (mg/g) at equilibrium, and  $k_1$  is the rate constant ( $\text{min}^{-1}$ ). Figure 7(a) shows the linear relation between  $\log(q_e - q_t)$  versus  $t$  with regression coefficient 0.975 and 0.980 for KZn and KCu, respectively.

The pseudo-second order equation can be expressed as following equations:

$$\frac{dq}{dt} = K_2 (q_e - q_t)^2 \quad (6)$$

$$\frac{t}{q_t} = \frac{1}{K_2 q_e^2} + \frac{1}{q_e} t \quad (7)$$

$k_2$  is the second-order rate constant of the adsorption process (g/mg. min).

Figure 7(b) shows the linear plots of  $t/q_t$  versus  $t$  with regression coefficients 0.992 and 0.996 for KZn and KCu, respectively. All kinetic parameters are calculated and listed in Table 1. Table 1 illustrates that the  $R^2$  % of the second order is higher than the  $R^2$  % of the first order, which indicates the well-fitting of the experimental results with second-ordered rather than first-ordered. Therefore the mechanism of the adsorption process of Th(IV) onto KZn and KCu is a chemisorption reaction.

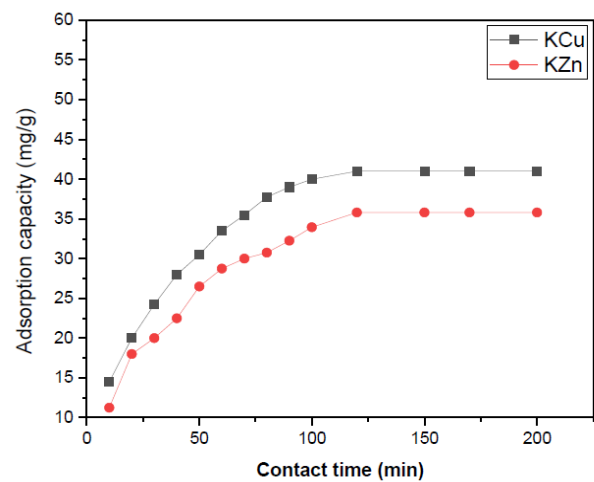


**Fig. (6): Effect of Contact time on Th(IV) adsorption on KCu and KZn, [  $C_0 = 50$  mg/L,  $m = 0.05$  g, pH=5 ]**

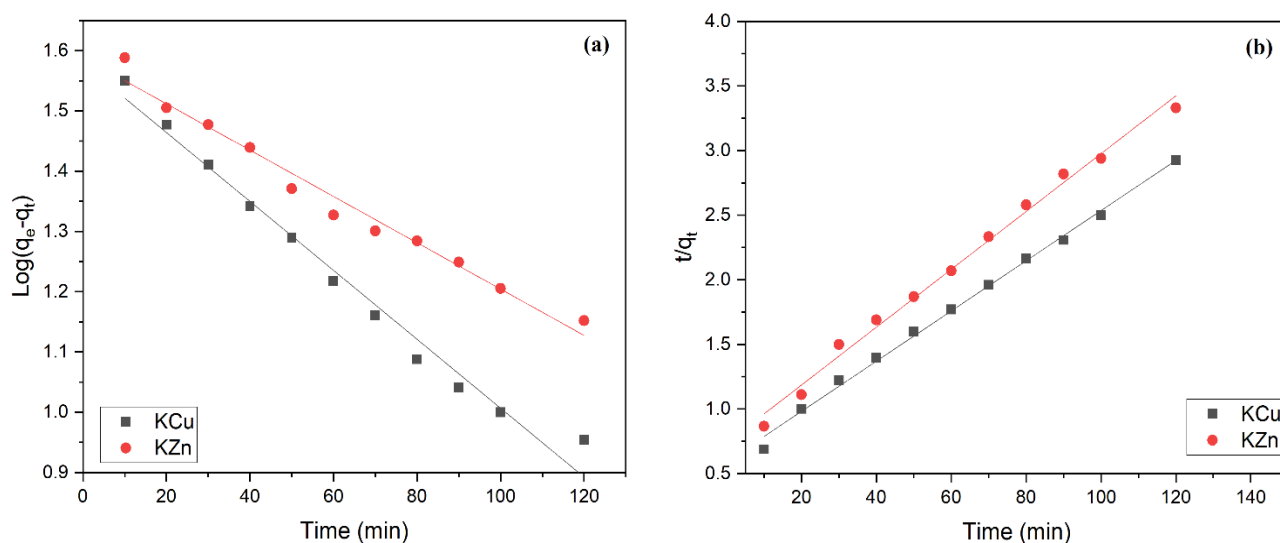


**Fig. (7): (a) Linear fit of pseudo first ordered kinetic model with the experimental data of Th(IV) adsorption on KCu and KZn; (b) Linear fit of pseudo second ordered kinetic model with the experimental data of Th(IV) adsorption on KCu and KZn**

**Table (1): Various adsorption kinetic parameters of Th(IV) adsorption on KCu and KZn**

Model	Parameters	KCu	KZn
Pseudo-first ordered	$K_1$ (1/min)	0.0131	0.0089
	$q_e$ (mg/g)	24.845	24.893
	$R^2$	0.980	0.975
Pseudo-second ordered	$K_2$ (g/mg. min)	$0.636 \times 10^{-3}$	$0.675 \times 10^{-3}$
	$q_e$ (mg/g)	51.546	44.483
	$R^2$	0.996	0.992

### 3.3. The effect of initial Th(IV) concentration and isothermal study

The effect of the initial concentration was investigated to study the isothermal model parameters. The adsorption process was carried out at a range of initial Th(IV) concentration 30-400 mg/L at 298 K. Figure 8 shows the effect of Th(IV) initial concentration on the equilibrium adsorption capacity  $q_e$  (mg/g) of Th(IV) on KZn and KCu. It was clear that  $q_t$  increases with the initial concentration of Th(IV) increased until reached saturation at 200 mg/g. Isothermal models are used to describe the mechanism of the adsorption reaction on the surface of the adsorbent by applying Langmuir and Freundlich models to the experimental data of the adsorption process [19]. The Langmuir isotherm model

describes the monolayer adsorption on a uniform surface. Only one layer of metal ions was adsorbed in each active site and no further adsorption can occur at this site. The linear form of the Langmuir isotherm model is described as the following [19]:

$$\frac{C_e}{q_e} = \frac{1}{K_L q_m} + \frac{C_e}{q_m} \quad (8)$$

Where  $C_e$  is the concentration of Th(IV) at equilibrium (mg/L),  $q_m$  is the maximum adsorption capacity (mg/g), and  $K_L$  is the Langmuir constant (L/mg). Figure 9 (a) shows the linear plots of Langmuir isotherm of Th(IV) adsorption on the KZn and KCu. The regression coefficient was  $R^2 = 0.994$  and  $0.993$  for KCu and KZn, respectively.

Freundlich isotherm applies to both multilayer chemisorption and multilayer physisorption based on the assumption that adsorption takes place onto the heterogeneous surface of an adsorbent. The linear form of the Freundlich equation is expressed as the following [20]:

$$\log q_e = \log K_F + \left(\frac{1}{n}\right) \text{Log } C_e \quad (9)$$

Where  $K_F$  is the Freundlich isotherm constant ( $\text{mg}^{1-1/n} \cdot \text{L}^{1/n/\text{g}}$ ),  $1/n$  is the heterogeneity factor constant related to surface heterogeneity [19]. Figure 9 (b) shows the linear plots of Freundlich isotherm of Th(IV) adsorption on the KCu and KZn. The regression coefficients are  $R^2 = 0.988$  and  $0.987$  for KCu and KZn, respectively. All isothermal model parameters are listed in Table 2. It indicates that the Langmuir isotherm model is fitted well with the experimental data more than the Freundlich isotherm model fitting. So, it may conclude that the equilibrium results of adsorption were best represented by the

Langmuir model, which indicates that the mechanism is a monolayer chemisorption adsorption reaction.

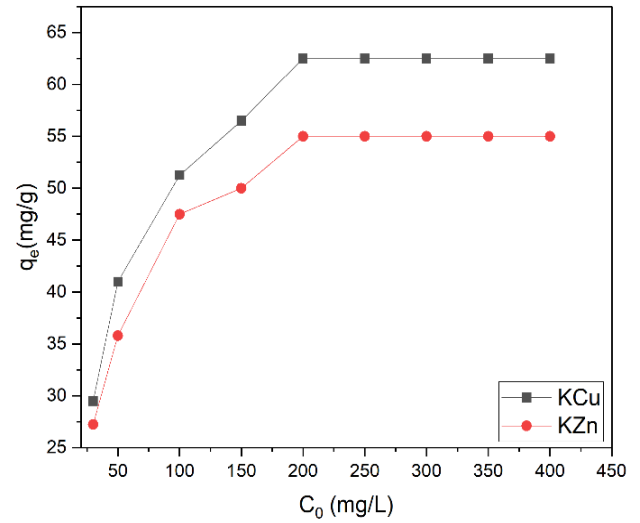


Fig. (8): Effect of Initial concentration of Th(IV) adsorption on KCu and KZn, [  $t=120$  min,  $m = 0.05$  g,  $\text{pH}=5$  ]

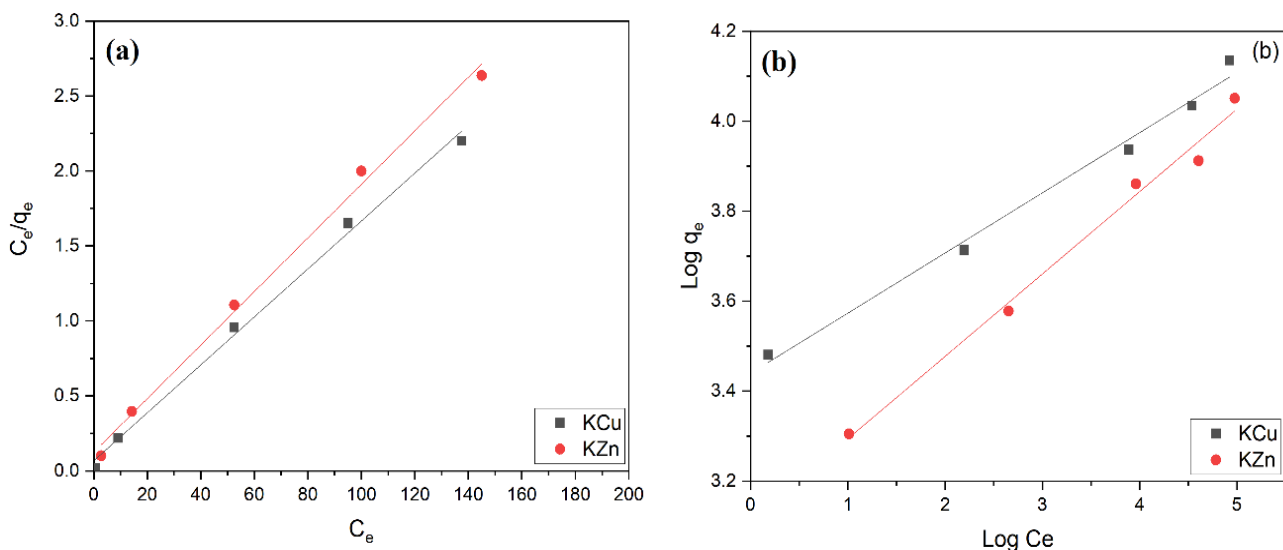


Fig. (9): (a) Langmuir linear plots for the adsorption of Th(IV) on KCu and KZn; (b) Freundlich linear plots for the adsorption of Th(IV) on KCu and KZn

Table (2): Various adsorption isothermal model parameters for Th(IV) adsorption on KCu and KZn

Adsorbent	Langmuir Isotherm Model			Freundlich Isotherm Model		
	$q_m$ (mg/g)	$k_l$ (L/ mg)	$R^2$	$K_F$ ( $\text{mg}^{1-1/n} \cdot \text{L}^{1/n/\text{g}}$ )	$1/n$	$R^2$
<b>KCu</b>	62.89	0.237	0.994	31.689	0.129	0.987
<b>KZn</b>	56.179	0.1435	0.993	22.421	0.183	0.988

### 3.4. The effect of temperature and thermodynamic study

The effect of temperature was investigated to study the thermodynamic model parameters. The adsorption process was carried out at an initial Th(IV) concentration of 50 mg/L at different temperatures 298, 308, 318, and 328 K. Thermodynamic parameters such as Gibbs free energy change  $\Delta G^\circ$  (kJ/ mol), entropy change  $\Delta S^\circ$  (J/ mol K), and enthalpy change  $\Delta H^\circ$  (kJ/ mol) were calculated using the Eqs. 10, 11, and 12 [21]:

$$\Delta G^\circ = -RT \ln K_d \quad (10)$$

$$\Delta G^\circ = \Delta H^\circ - T\Delta S^\circ \quad (11)$$

$$\ln K_d = \frac{\Delta S^\circ}{R} - \frac{\Delta H^\circ}{RT} \quad (12)$$

$K_d$  (L/g) is the equilibrium constant, and  $R$  is the gas constant (8.314 J/ mol K). Figure 10 shows the linear plot of  $\ln K_d$  versus  $1/T$  to identify entropy and enthalpy changes. All isothermal parameters are listed in Table 3. From the data illustrated in Table 3, the positive value of  $\Delta H^\circ$  and the negative value of  $\Delta G^\circ$  indicates the adsorption of Th(IV) onto KZn and KCu was

endothermic and spontaneous. The positive value of  $\Delta S^\circ$  showed increased randomness at the solid–solution interface during the adsorption process [22].

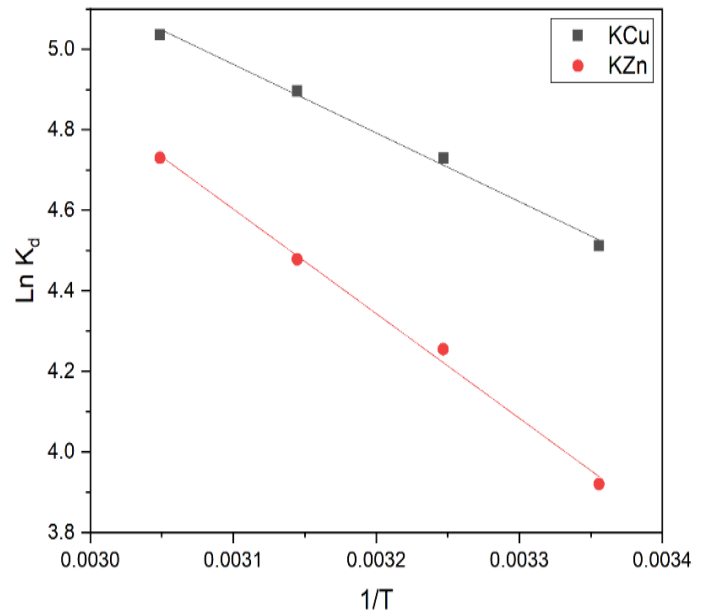


Fig. (10): Effect of temperature on the adsorption of Th(IV) on KCu and KZn

Table (3): Various adsorption thermodynamic parameters for Th(IV) adsorption on KCu and KZn

Adsorbent	Temperature (K)	$\ln K_d$ (mL/g)	$\Delta G^\circ$ (KJ/mol)	$\Delta S^\circ$ (J/mol K)	$\Delta H^\circ$ (kJ/mol)	Adj. $R^2$
KCu	298	4.512	-11.179	85.16	14.158	0.991
	308	4.730	-12.113			
	318	4.896	-12.946			
	328	5.036	-13.734			
KZn	298	9.492	-9.713	105.17	21.583	0.993
	308	9.9307	-11.063			
	318	10.399	-11.840			
	328	10.8097	-12.899			

### 3.5. Regeneration and reusability study

The regeneration and reusability of the adsorbent are important aspects in investigating the economic value of using the prepared adsorbent in the adsorption process. Recover Th(IV) from KZn and KCu was carried out in batch experiments using 0.01 M HCl that repeated five cycles. The experimental adsorption capacities were decreased by < 6 % after five cycles of Th(IV) adsorption within the same experimental conditions considered in this work at 298 K. Therefore, the reusability study considers that KZn and KCu are efficient and economical for removing Th(IV) from aqueous solution.

## 4. CONCLUSIONS

In this work, Egyptian natural kaolinite is supported with copper and zinc oxides to form the new adsorbents KCu and KZn, respectively. The modified adsorbents KZn and KCu were prepared by calcination in a muffle furnace at 700 °C. Modified adsorbents were characterized by different techniques: SEM, EDX, XRD, and FTIR. The newly modified kaolinites were employed to adsorb Th(IV) from an aqueous solution. The experimental data fits well with the pseudo-second-order and the Langmuir models explain the monolayered chemisorption mechanism of the adsorption process. The removal of Th(IV) from the aqueous solution was favorable by increasing temperature, indicating the endothermic nature of the adsorption process. Thermodynamics studies confirmed that adsorption is feasible and spontaneous. The regeneration and reusability study showed that KZn and KCu are economically viable.

## 5. REFERENCES

- [1] Qi C., Liu H., Deng S., Yang A., Li Z. (2018) A modeling study by response surface methodology (RSM) on Th(IV) adsorption optimization using a sulfated  $\beta$ -cyclodextrin inclusion complex, *Res Chem Intermed.*, **44**, 2889–2911, <https://doi.org/10.1007/s11164-018-3286-3>.
- [2] Wang Y., Chen X., Hu X., Wu P., Lan T., Li Y., Tu H., Liu Y., Yuan D., Wu Z., Liu Z., Chew W. (2021) Synthesis and characterization of poly(TRIM/VPA) functionalized graphene oxide nanoribbons aerogel for highly efficient capture of thorium(IV) from aqueous solutions, *Appl. Surf. Sci.* **536**, 147829.
- [3] Deb A., Mohanty B. N., Ilaiyaraja P., Sivasubramanian K., Venkatraman B. (2013) Adsorptive removal of thorium from aqueous solution using diglycolamide functionalized multi-walled carbon nanotubes. *J Radioanal Nucl Chem.*, **295**, 1161–1169, [DOI 10.1007/s10967-012-1899-3](https://doi.org/10.1007/s10967-012-1899-3).
- [4] Radchenko V., Engle J. W., Wilson J. J., Maassen J. R., Nortier F. M., Taylor W. A., Birnbaum E. R., Hudston L.A., John K.D., Fassbender M.E. (2015) Application of ion exchange and extraction chromatography to the separation of actinium from proton-irradiated thorium metal for analytical purposes., *J. Chromatogr A.*, **13** (80) 55–63.
- [5] Al Abdullah J., Al Laf A., Al Masri W., Amin Y., Alnana T. (2016) Adsorption of cesium, cobalt, and lead onto a synthetic nano manganese oxide: behavior and mechanism. *Water Air Soil Pollut.*, **227**, 1–14.
- [6] Shaeri M., Torab-Mostaedi M., Kelishami A.R. (2015) Solvent extraction of thorium from nitrate medium by TBP, Cyanex272 and their mixture. *J. Radioanal Nucl Chem.*, **303** (6) 2093–2099.
- [7] Al Lafi A. G., Ajji Z. (2017) Radiation grafting of acrylic acid and N-vinyl imidazole onto polyethylene films for lead-ion removal: a two-dimensional correlation infrared spectroscopy investigation., *J. Appl. Polym Sci.*, **134**, 44781.
- [8] Uehara A., Fujii T., Yamana H., Okamoto Y. (2016) An in-situ x-ray absorption spectroelectrochemical study of the electroreduction of uranium ions in HCl, HNO<sub>3</sub>, and Na<sub>2</sub>CO<sub>3</sub> solutions. *Radiochim. Acta*, **104**, 1–9.
- [9] Xiu T., Liu Z., Yang L., Wang Y. (2019) Removal of thorium and uranium from aqueous solution by adsorption on hydrated manganese dioxide, *Journal of Radioanalytical and Nuclear Chemistry*, **321**, 671–681, <https://doi.org/10.1007/s10967-019-06634-2>.
- [10] Zhou L., Wang Y., Zou H., Liang X., Zeng K., Liu Z., Adesina A.A. (2016) Biosorption characteristics of uranium (VI) and thorium (IV) ions from aqueous solution using CaCl<sub>2</sub>-modified Giant Kelp biomass, *J. Radioanal Nucl Chem.*, **307** (1) 635–644.
- [11] Nilchi A., Dehaghan T.S., Garmarodi S.R. (2013) Solid phase extraction of uranium and thorium on octadecyl bonded silica modified with Cyanex 302

- from aqueous solutions, *J. Radioanal Nucl Chem.*, **295** (3) 2111–2115.
- [12] Sarafraz H., Minuchehr A., Alahyarizadeh G., Rahimi Z. (2017) Synthesis of enhanced phosphonic functional groups mesoporous silica for uranium selective adsorption from aqueous solutions. *Sci Rep.*, **7**, 11675–11682.
- [13] Feriancova A., Pajtašova M., Palieskova J., Ondrušova D., Kopicova M., Joňáková E., Mojumdar S. C. (2013) The influence of kaolin filler on thermal and spectral characteristics of rubberizing components without rubber, *J Therm Anal Calorim.*, **112**, 1047–1052, [DOI 10.1007/s10973-013-3060-0](https://doi.org/10.1007/s10973-013-3060-0).
- [14] Fida H., Guo S., Zhang G. (2015) Preparation and characterization of bifunctional Ti–Fe kaolinite composite for Cr(VI) removal., *J. Colloid Interf. Sci.* **442**, 30.
- [15] Elhefnawy O. A., Elabd A. A., (2017) Optimization of uranyl ions removal from aqueous solution by natural and modified Kaolinites, *Radiochim Acta*; **105**(8) 609–620, [DOI: 10.1515/ract-2016-2712](https://doi.org/10.1515/ract-2016-2712).
- [16] Kanani M.V., Dhruv D., Rathod H. K., Rathod K.N., Rajyaguru B., Joshi A.D., Solanki P.S., Shah N.A., Pandya D.D. (2019) Investigations on structural, optical and electrical property of ZnO–CuO core–shell nano-composite, *Scripta Materialia*, **165**, 25–28.
- [17] Elhefnawy O. A., and Elabd A. A. (2022) Effective adsorption of U(VI) from aqueous solution using polystyrene grafted with zeolite, *Pigment & Resin Technology*, [DOI 10.1108/PRT-02-2022-00211](https://doi.org/10.1108/PRT-02-2022-00211).
- [18] Ganguly P., Sarkhel R., Das P., (2020) Synthesis of pyrolyzed biochar and its application for dye removal: batch, kinetic and isotherm with linear and non-linear mathematical analysis, *Surf Interfaces.*, **20**, 100616. <https://doi.org/10.1016/j.surfin.2020.100616>.
- [19] Elhefnawy O. A., and Elabd A. A., (2022) Adsorption of  $UO_2^{2+}$  by AlBaNi-layered double hydroxide nano-particles: kinetic, isothermal, and thermodynamic studies, *Radiochim. Acta*; **110** (3) 173–183.
- [20] Nnadozie E. C., Ajibade P.A., (2020) Data for experimental and calculated values of the adsorption of Pb(II) and Cr(VI) on APTES functionalized magnetite biochar using Langmuir, Freundlich and Temkin equations. *Data Brief.*, **32**, 106292. <https://doi.org/10.1016/j.dib.2020.106292>.
- [21] Xiu T., Liu Z., Wang Y., Wu P., Du Y., Cai Z. (2019) Thorium adsorption on graphene oxide nanoribbons/manganese dioxide composite material. *J. Radioanal. Nucl. Chem.*, **319**, 1059–1067.
- [22] Elhefnawy, O. A., and Elabd, A. A., (2022) Preparation and characterization of core-shell structured nanocomposite materials and their adsorption behavior on U (VI) from aqueous solutions, *Appl Organomet Chem.*, **37** (2) 6928, <https://doi.org/10.1002/aoc.6928>.